

# Influence of eigenmode characteristics on optical tuning of a two-dimensional silicon photonic crystal

H. W. Tan and H. M. van Driel

*Department of Physics and Institute for Optical Sciences, University of Toronto, Toronto, Ontario, Canada M5S 1A7*

S. L. Schweizer and R. B. Wehrspohn

*Nanophotonics Materials Group, Department of Physics, University of Paderborn, 33095 Paderborn, Germany*

(Received 15 February 2005; revised manuscript received 5 July 2005; published 28 October 2005)

Ultrafast pump-probe measurements on a two-dimensional (2-D) silicon photonic crystal are used to show the influence of a pump eigenmode's spatial characteristics on the crystal's optical tuning properties. Electron-hole pairs are generated by two-photon absorption of 130 fs, 1.5  $\mu\text{m}$  pulses via different crystal eigenmodes and spatially modify the crystal's refractive index via Drude effects; characteristics of an eigenmode near 1.9  $\mu\text{m}$  are monitored via time-resolved reflectivity. For a pump eigenmode producing an inhomogeneous carrier distribution, diffusion is responsible for an initially fast (10 ps time scale) component of the recovery of the probe reflectivity with surface recombination accounting for a slower response (700 ps time scale) after the carriers are nearly uniformly distributed within the silicon backbone. When carriers are initially generated homogeneously in the silicon, surface recombination alone controls the time evolution of the probed mode. A simple expression is developed for the mode-dependent two photon absorption in photonic crystals and a simple perturbation technique is used to treat modifications to photonic crystal eigenmodes by small refractive index changes.

DOI: [10.1103/PhysRevB.72.165115](https://doi.org/10.1103/PhysRevB.72.165115)

PACS number(s): 42.70.Qs, 42.65.Re, 42.65.Sf

## I. INTRODUCTION

Tuning of the optical properties of a photonic crystal (PhC) has been the subject of intense research efforts related to the potential development of active photonic crystal components. With femto- or picosecond pulse excitation of PhCs, tuning is usually achieved via the free-carrier-induced Drude effect or the Kerr effect.<sup>1-6</sup> However, little attention has been paid to how the spatial characteristics of the excited eigenmodes influence the temporal or spectral dependence of the optical response. In this paper we report the results of experiments in which 1.5  $\mu\text{m}$ , 130 fs pulses excite carriers in a two-dimensional (2D) silicon PhC by two photon absorption (2PA) via PhC eigenmodes with different spatial characteristics. We demonstrate a time- and pump mode-dependent modification of the silicon refractive index via the Drude effect and monitor this using time-resolved reflectivity in the vicinity of a PhC mode at 1.9  $\mu\text{m}$ . The 2PA absorption depth is sufficiently large that a mode description of the initial carrier description is possible. A simple perturbation technique<sup>7</sup> is adapted to determine how PhC eigenfrequencies in general are influenced by small, refractive index changes in the PhC. The degree of tuning is controlled by the spatial overlap of the induced refractive index change (governed by the pump mode) with the probe mode energy density.

Although the generated carriers are initially distributed according to the pump mode (actually the fourth power of the mode's field distribution for 2PA), this distribution can be influenced by disorder within the PhC but not appreciably affected by surface termination and weak beam focusing. Subsequently, the dynamics and spatial distribution of the carriers are governed by diffusion as well as surface and bulk

recombination. Owing to the fact that bulk recombination in defect-free Si is slow and carriers are generated within hundreds of nanometers of a surface, surface recombination is found to dominate bulk recombination.<sup>8</sup>

The PhC sample used for the experiments is similar to that described elsewhere.<sup>4</sup> As shown in Fig. 1 the silicon sample has a triangular lattice arrangement of 560 nm diameter, 96  $\mu\text{m}$  deep air holes with a pitch of 700 nm. Figure 2 shows the calculated photonic band structure for light propagating along the  $\Gamma$ - $M$  direction, which is normal to a face of the PhC. The pump modes labeled (A)-(D) at  $0.25k_0$ ,  $0.5k_0$ ,  $0.75k_0$ , and  $k_0$  (where  $k_0$  is the  $\Gamma$ - $M$  wave vector) are used to make specific comparisons later in the text. Experimentally, the optical tuning of the PhC was accomplished using a parametric amplifier pumped by a 250 kHz repetition rate Ti-sapphire oscillator/regenerative amplifier. The 1.5  $\mu\text{m}$ , 130 fs signal (pump) pulses are focused onto the sample with a spot size of 34  $\mu\text{m}$  (FWHM) and a peak intensity of 16  $\text{GW}/\text{cm}^2$ . The pump beam can be introduced either along the  $\Gamma$ - $M$  direction (the  $z$  direction of Fig. 1), with the E-field

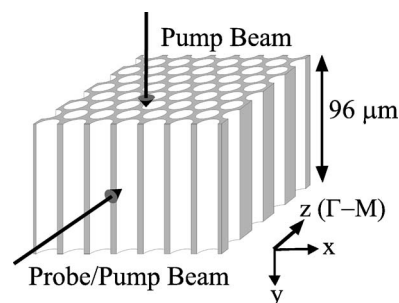


FIG. 1. Schematic diagram of the 2-D silicon photonic crystal with an axis reference system.

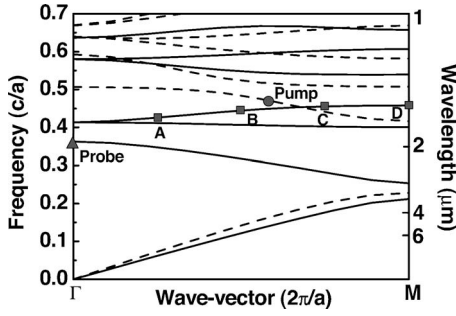


FIG. 2. Dispersion curves of the 2D silicon PhC for the  $\Gamma$ - $M$  direction. The solid and dashed lines correspond to E- and H-polarized light, respectively. The filled triangle and circle correspond to the experimental probe and pump frequencies, respectively. The filled squares (A)–(D) indicate the pump frequencies used in some of the simulations.

polarized normal to the pore axis or near the front face of the PhC, along the pore-axis direction (the  $y$  direction in Fig. 1) with the E-field polarized along the  $\Gamma$ - $M$  direction. The 2PA of the pump pulses generate free carriers that induce a change in the refractive index of the silicon. The subsequent tuning of the photonic band structure is probed via reflectivity of a weak, E-polarized (i.e., polarized along the  $y$  direction)  $1.9 \mu\text{m}$  idler beam that has a focused spot size of  $20 \mu\text{m}$  and a peak intensity of  $0.2 \text{ GW}/\text{cm}^2$ . This probe beam is incident along the  $\Gamma$ - $M$  direction and tuned to the longer-wavelength band edge of the second stop gap that is sensitive to small changes in the Si refractive index.

## II. THEORETICAL CONCEPTS

Mode frequency shifts that result from weak changes in the index of refraction can be derived using perturbation theory, using an approach similar to that used in elementary quantum mechanics.<sup>7</sup> We consider a PhC characterized by a position-dependent index of refraction  $n(\mathbf{r})$  with modes labeled by crystal momentum  $\mathbf{k}$  and band index  $m$ . For a non-degenerate mode with frequency  $\omega_{m\mathbf{k}}$ , under a (periodic) change in the index of refraction with  $n(\mathbf{r}) \rightarrow n(\mathbf{r}) + \Delta n(\mathbf{r})$ , to lowest order in  $\Delta n(\mathbf{r})$  a mode frequency changes according to  $\omega_{m\mathbf{k}} \rightarrow \omega_{m\mathbf{k}} + \Delta\omega$ , where

$$\frac{\Delta\omega}{\omega_{m\mathbf{k}}} = - \frac{\int_{\text{cell}} \frac{\Delta n(\mathbf{r})}{n(\mathbf{r})} U_{m\mathbf{k}}(\mathbf{r}) d\mathbf{r}}{\int_{\text{cell}} U_{m\mathbf{k}}(\mathbf{r}) d\mathbf{r}}, \quad (1)$$

and

$$U_{m\mathbf{k}}(\mathbf{r}) \equiv \varepsilon_0 n^2(\mathbf{r}) \mathbf{E}_{m\mathbf{k}}^*(\mathbf{r}) \cdot \mathbf{E}_{m\mathbf{k}}(\mathbf{r})$$

identifies the spatially dependent, time-averaged energy density distribution associated with the mode  $m\mathbf{k}$  and electric field spatial profile  $\mathbf{E}_{m\mathbf{k}}(\mathbf{r})$ . Since both  $U_{m\mathbf{k}}(\mathbf{r})$  and  $\Delta n(\mathbf{r})$  are periodic in the PhC, the integrals in Eq. (1) extend only over a unit cell. The  $U_{m\mathbf{k}}(\mathbf{r})$  or the  $\mathbf{E}_{m\mathbf{k}}(\mathbf{r})$  are determined from the PhC eigenmode equations. Note that the result in Eq. (1) is

independent of the normalization chosen for  $\mathbf{E}_{m\mathbf{k}}(\mathbf{r})$ .

In addition to using result (1) to determine mode shifts, we employed finite difference time domain (FDTD) techniques to determine if the pulsed excitation of the PhC produces effects that differ from continuous (time-independent) excitation, as assumed above. In the FDTD calculations a  $1.5 \mu\text{m}$ , 130 fs pump pulse is launched from air into a PhC that is treated as periodic in the  $x$  direction but has a finite length of 30 rows along the  $z$  direction. This sample length is chosen so that the pulse does not reach the end of the sample before the power distribution is determined; this prevents any interference from backreflected fields. The FDTD calculations show that the power distributions are not changed significantly by surface termination, even though the sample transmissivity may be strongly affected.<sup>9</sup> At normal incidence, these distributions are established once the pulse enters the samples and show little variation for incident angles up to 10 deg. Slight deviations occur only in the first crystal row at the sample edge because slightly off-normal incidence beams are refracted toward the normal, taking into account the band structure of the PhC.<sup>10</sup> Since the focused beams converge with an angle  $< 4$  deg on the sample, we do not expect significant deviations from the calculated power distributions from focusing effects. We also verified that the energy density distributions are not appreciably affected by weak absorption, e.g., owing to 2PA in the silicon backbone.

A simple model<sup>11</sup> is used to describe the generation and evolution of a spatially inhomogeneous carrier distribution within the PhC backbone. The carrier density evolution can be described by

$$\frac{\partial N(\mathbf{r})}{\partial t} = D_N \nabla^2 N + \left. \frac{\partial N}{\partial t} \right|_{\text{gen}}, \quad (2)$$

where  $D_N = 10 \text{ cm}^2/\text{s}$  is taken to be the ambipolar diffusivity<sup>12,13</sup> appropriate for our typical carrier density ( $\sim 10^{18} \text{ cm}^{-3}$ ) and “gen” refers to a carrier generation process. The time constants associated with radiative and Auger recombination for this density are 17 and  $2.5 \mu\text{s}$ , respectively, and are assumed to be negligible in our experiments, where the characteristic evolution time scale is  $< 1$  ns. We furthermore assume that the recombination time associated with bulk defects and impurities in the high-quality silicon backbone is  $\gg 1$  ns since the bulk resistivity is  $40 \Omega \text{ cm}$ , with an  $n$ -doping density of  $\sim 10^{15} \text{ cm}^{-3}$ .<sup>14</sup> Recombination in these macroporous samples is likely dominated by surface effects. For a surface recombination velocity  $S$ , one has the boundary condition

$$S N(\mathbf{r}, t)|_{\text{surface}} = D_N |\nabla N|_{\text{surface}}. \quad (3)$$

In our experiments in which carriers are excited via 2PA, the carrier generation term becomes

$$\left. \frac{\partial N}{\partial t} \right|_{\text{gen}} = \frac{\beta(\mathbf{r}, \omega_p)}{2\hbar\Omega} I^2(\mathbf{r}, t), \quad (4)$$

where  $\omega_p$  refers to the pump frequency,  $I(\mathbf{r}, t)$  is the intensity at location  $\mathbf{r}$  inside the photonic crystal, and  $\beta(\mathbf{r}, \omega_p)$  is the local 2PA coefficient. For our peak intensities the absorption depth associated with 2PA is  $\gg 1 \mu\text{m}$  and 2PA does not sig-

nificantly alter the PhC modes, including their lifetime. However, the field distribution of the excited mode can influence the local carrier generation rate. Also, the group velocity<sup>15</sup> of the pump beam eigenmode can differ from that in bulk silicon. In the Appendix we derive the local 2PA coefficient inside the PhC in terms of mode characteristics. For our purposes here, with light polarized along one of the silicon principal axes (also parallel or perpendicular to the cylinder axis), we can neglect the anisotropy characteristics of 2PA and use the effective 2PA coefficient given by Eq. (15).

Equations (2) and (3) can be numerically solved for  $N$ , with the initial condition that the quiescent carrier density in the silicon is  $10^{15} \text{ cm}^{-3}$ . A unit cell of the PhC is divided into a spatial grid and the carrier evolution equations are discretized within the silicon backbone via a forward time-centered space scheme.<sup>16</sup> Periodic boundary conditions are assumed, reflecting the translational symmetry of the PhC. The induced refractive index change is given by<sup>17</sup>

$$\Delta n(\mathbf{r}, t) = -\frac{e^2}{2nm^* \epsilon_0 \omega_r^2} N(\mathbf{r}, t), \quad (5)$$

where  $m^* = 0.16m_0$  is the optical effective mass of the electrons and holes, and  $\omega_r = 2.87 \times 10^{14} \text{ rad/s}$  is the probe frequency. Equation (5) can be substituted into Eq. (1) to compute the frequency shift for a mode at different probe delays. Because the pump pulse width is much less than the time scale on which diffusion and surface recombination occur, the carriers can be considered to have been injected at  $t=0$ . Furthermore, the time scale on which the mode frequencies change is long compared to the inverse of the mode frequency so that the induced shift can be regarded as a steady-state response.

To illustrate how spatial overlap between the pump and probe pulses influences tuning, we have simulated the shift in the  $1.9 \mu\text{m}$  band edge when the PhC is pumped with 130 fs pulses with a center wavelength between 1.1 and  $2.2 \mu\text{m}$ , a wavelength range over which 2PA may occur in silicon. Here, the E-polarized pump and probe beams are incident along the  $\Gamma$ - $M$  direction of the PhC and the 2PA coefficient is treated as frequency independent to elucidate the role of the modes. For carriers generated via 2PA,  $\Delta n(\mathbf{r})$  is proportional to the square of the local pump energy density. Figure 3 shows the frequency shift at the probe mode immediately after the pump pulse for various pump modes [including the (A)–(D) modes of Fig. 2] calculated using Eq. (1). The pump modes chosen are those that can be optically excited by incident plane waves. The pump pulse intensity is chosen to produce the same *average* carrier density in the silicon, although the density varies in space according to the pump mode spatial profile. The shifts plotted are those that would be recorded before diffusion or recombination alter the injected carrier density, i.e., on a picosecond time scale. Under the conditions stated, one obtains a significant variation in the  $1.9 \mu\text{m}$  mode with an excitation mode. While the shifts plotted are given in arbitrary units, it might be pointed out that typical shifts are of the order of several nm for an average injected carrier density of  $\sim 10^{18} \text{ cm}^{-3}$ , similar to

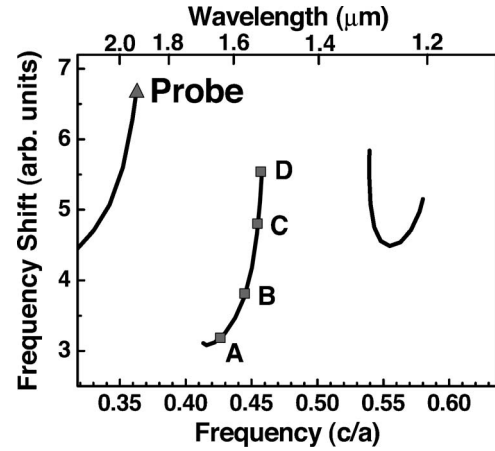


FIG. 3. Magnitude of induced mode tuning at  $1.9 \mu\text{m}$  as a function of pump wavelength for the same, average carrier density in the silicon backbone. Both the E-polarized pump and probe beams are incident along the  $\Gamma$ - $M$  direction. The filled squares (A)–(D) indicate the pump frequencies used in some of the simulations while the filled triangle indicates the  $1.9 \mu\text{m}$  probe wavelength used in the experiments.

experimental results obtained by Leonard *et al.*<sup>4</sup> Consistent with Eq. (1) we find that the largest frequency shift is achieved when the spatial overlap between  $U_{mk}(\mathbf{r})$  and  $\Delta n(\mathbf{r})$  is large, i.e., when the pump and probe beams are degenerate or nearly so. Similar results are also obtained for  $H$ -polarized pump light. This is clearly illustrated in Fig. 4, which shows the energy density of the (A)–(D) modes located on a relatively flat dispersion curve. Also shown in Fig. 4 is the energy density of the probe mode [labeled (E)]. A comparison of Figs. 3 and 4 shows how the frequency shift varies with pump mode/probe mode overlap. In the experiments, rather than directly observing the frequency shift of a  $1.9 \mu\text{m}$  mode, which defines one edge of a photonic band gap, we measure the change of the reflectivity ( $R$ ) at the corresponding Bragg reflectivity peak, making use of the fact that  $\Delta R = (\partial R / \partial \omega) \Delta \omega$ .

Although we do not consider this explicitly here, another method for inducing a mode frequency shift is through a Kerr-induced refractive index change.<sup>18</sup> The treatment of this spatially dependent effect is similar to that of the 2PA process, as shown in the Appendix, although as is well known<sup>4</sup> for a given laser intensity, Kerr-induced changes are much smaller than Drude-induced changes. The tradeoff is that for the Kerr effect the induced changes follow the optical pulse temporal profile.

### III. EXPERIMENTAL RESULTS AND DISCUSSION

Figure 5(a) shows the experimental time-resolved probe reflectivity results and curves derived from simulations based on Eq. (1) for the two different pump geometries. When the pump beam is incident along the  $\Gamma$ - $M$  direction, there is partial recovery in the probe reflectivity on a 10 ps time scale followed by a slower recovery on a few hundred picosecond time scale. When the pump propagates along the pore axis, the probe reflectivity recovers with a 700 ps time constant.

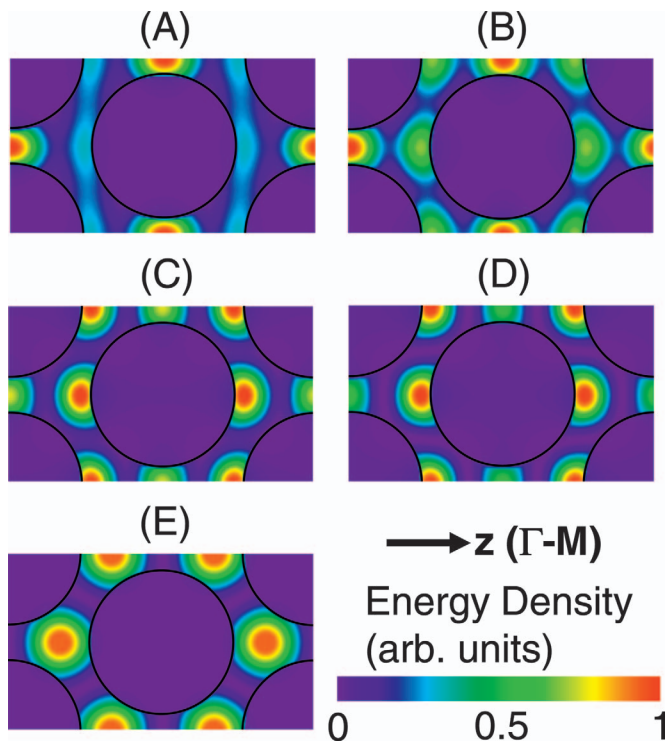


FIG. 4. (Color) Spatial energy density distributions corresponding to the (A)–(D) modes shown in Fig. 2; (E) shows the energy density distribution for the eigenmode probed in the experiments.

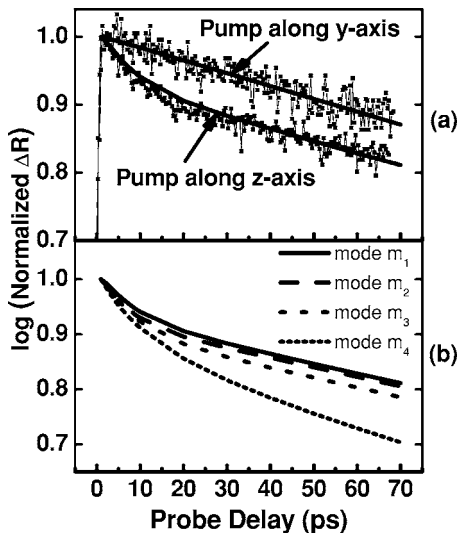


FIG. 5. Time dependence of normalized reflectivity change for two different pump-probe geometries. In (a), the filled squares are the experimental data points and the bold lines are the fitted curves in a sample that has 560 nm diameter air holes with a pitch of 700 nm. The pump eigenmode is excited by 1.5  $\mu\text{m}$ , H-polarized light. In (b), simulation results are shown for different pump modes in two different samples. The trace corresponding to mode  $m_1$  is the same as the lower trace in (a). Modes  $m_2$  and  $m_3$  are excited by E- and H-polarized, 1.25  $\mu\text{m}$  light, respectively, in the same sample. Mode  $m_4$  is excited by 1.5  $\mu\text{m}$ , E-polarized light in a PhC that has 400 nm diameter air holes with a pitch of 500 nm.

The difference in the temporal dependence of the reflectivity can be attributed to the different initial spatial distributions of the free carriers, although in both cases smearing of the mode field distribution by defects in the PhC can influence the corresponding carrier distributions. This might be expected to be more important when the pump propagates along the pore axis since it must propagate  $\sim 50 \mu\text{m}$  in the PhC before it reaches the probe location. At such a depth the carriers could be expected to be almost uniformly distributed within the silicon and carrier evolution would occur via recombination alone. However, if the pump and probe beams propagate collinearly along the  $\Gamma$ - $M$  direction, the sampled carrier distribution will not differ significantly from that in a perfect PhC sample since the effective probe depth is limited to the first few PhC unit cells.<sup>19</sup> The measured reflectivity results are therefore influenced by both carrier diffusion and recombination.

In the simulations, since the free carriers are generated by 2PA of the pump pulse, their initial distributions  $N(x, z, t = 0)$  can be inferred by taking the square of the energy density  $U_{mk}(r)$  at the pump frequency in the silicon backbone. For the pump beam incident along the pore axis direction, the initial carrier distribution is assumed to be uniform in the silicon. The solutions for  $N(x, z, t)$  obtained by solving Eq. (2) and Eq. (3) are substituted into Eq. (1) to compute the band-edge shifts at different probe delays. For small index changes, the reflectivity change is proportional to the band-edge shifts. It should also be noted that  $S$  is the only free parameter used to fit the simulation traces to the experimental data.

The best fit results, obtained for  $S = 7 \times 10^4 \text{ cm/s}$ , are shown in Fig. 5(a) and show reasonable agreement. In high-quality crystalline Si, the value of  $S$  has been measured to be  $3 \times 10^4 \text{ cm/s}$  but can be as large as  $10^6 \text{ cm/s}$  as the surface quality degrades.<sup>20</sup> When the pump direction lies along the  $\Gamma$ - $M$  direction and the initial carrier distribution is inhomogeneous in the PhC, carrier diffusion accounts for the initial fast recovery in the reflectivity traces. The initial contrast between the regions of high and low carrier density is also accentuated by the 2PA process. After the carriers are uniformly distributed after  $\sim 30 \text{ ps}$ , the recovery is slower and can be attributed to surface recombination.<sup>21</sup> When the pump beam is incident along the pore axis, the uniform carrier distribution decays via surface recombination alone. This re-

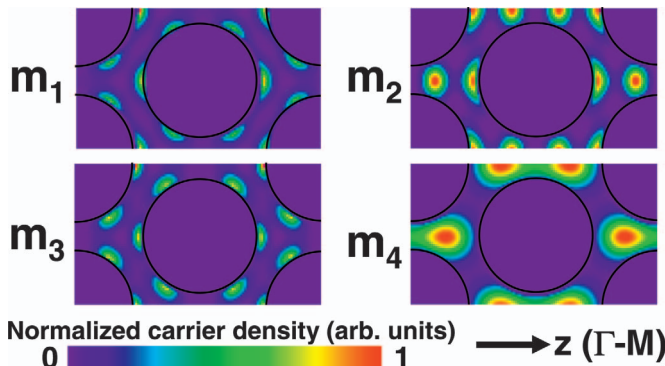


FIG. 6. (Color) Initial free carrier distributions (shaded areas) for pump modes  $m_1$  to  $m_4$ .

sult is also consistent with earlier results obtained when a  $1.76 \mu\text{m}$  pump beam, also introduced along the pore axis, was used to tune the  $1.6 \mu\text{m}$  band edge for E-polarized light in the same sample.<sup>22</sup> Note that the subnanosecond carrier surface recombination time can be estimated from Eq. (3) (since both terms represent current density into the interface) as  $L/S$ , where  $L$  is the thickness of the Si neck; For  $L = 0.2 \mu\text{m}$ ,  $L/S \sim 300 \text{ ps}$ . In general, the time constant is independent of the diffusion coefficient, which simply governs the size of the (weak) density gradient. Although the possible temporal dependence of  $S$  on a picosecond time scale due to surface charging and the transient occupation of surface states<sup>23,24</sup> has been neglected in our simulations, the model describes the experimental results reasonably well. There is a noticeable discrepancy between the simulation and experimental results for the collinear pump-probe geometry. This could be reduced by employing a diffusion coefficient of  $20 \text{ cm}^2 \text{ s}^{-1}$ , however, it might be misleading to do so since part of the discrepancy may reflect other effects such as a different initial carrier distribution owing to PhC or mode imperfections, including clipped pore effects near the surface. The experimental results also reflect averaging effects related to pump and probe volumes.

To illustrate the influence different excited modes can have on the dynamics of the injected free carriers, simulations were also carried out using different pump wavelengths and a different PhC pitch. Figure 5(b) shows the results of these simulations for  $D_N = 10 \text{ cm}^2/\text{s}$  and  $S = 7 \times 10^4 \text{ cm/s}$ ; four modes,  $m_1, \dots, m_4$ , were considered. The corresponding initial free carrier distribution for these modes is illustrated in Fig. 6. Mode  $m_1$  is the same as the one used as a probe mode and the simulation trace is the same as the lower one in Fig. 5(a). Modes  $m_2$  and  $m_3$  are excited by E- and H-polarized,  $1.25 \mu\text{m}$  pump beams, respectively, incident along the  $\Gamma$ - $M$  direction in a sample of the same characteristics as was used in the experiments.<sup>25</sup> Although the initial free carrier distribution patterns for modes  $m_3$  and  $m_1$  are very similar (the modes lie on different air bands), the initial carrier density gradient is larger in the former case. This results in stronger carrier diffusion and thus faster recovery, as shown in Fig. 5(b). It is also interesting to note that although the field distributions for mode  $m_2$  and  $m_1$  are very different, their corresponding reflectivity traces are similar. It is thus difficult for one to conclusively differentiate the various mode excitations based on the time-dependent reflectivity traces alone. The curve corresponding to mode  $m_4$  in Fig. 5(b) is the result obtained when an E-polarized,  $1.5 \mu\text{m}$  pump beam is incident along the  $\Gamma$ - $M$  direction of a PhC but with  $400 \text{ nm}$  diameter air holes and a pitch of  $500 \text{ nm}$ . The reflectivity recovery is found to be faster in this material, although it has the same radius to pitch ratio as the one used in the experiment. This is due to the different initial carrier distributions and also the larger surface area to volume ratio (factor of 1.4) of the sample that results in the enhancement of the role played by surface recombination. Therefore, a complete picture of the probe reflectivity recovery must also include considerations of the PhC sample geometry. Indeed, it may be simpler to experimentally observe enhanced surface recombination effects from samples with different pitch than from attempts to differentiate the different pump modes in samples with the same pitch.

#### IV. CONCLUSIONS

We have shown that the field distributions of optical pump pulses in PhCs can influence both the magnitude and temporal characteristics of optical tuning through differences in the dynamics of the generated free carriers. The interplay between carrier diffusion and surface recombination is responsible for the overall temporal dynamics and surface recombination becomes even more important when the surface area to volume ratio of the sample is increased. While the results here point out how pump mode characteristics are important in determining dynamical optical effects in photonic crystals, the inverse problem, namely determining the spatial characteristics of an induced refractive index change in a photonic crystal from the time-dependent optical properties, does not present a unique solution in general.

#### ACKNOWLEDGMENTS

H.W.T. and H.v.D. gratefully acknowledge the financial support of Photonics Research Ontario and the Natural Sciences and Engineering Research Council and helpful discussions with John Sipe about nonlinear effects in photonic crystals. R.B.W. thanks the DFG in the SPP 1113 under WE 2637/3.

#### APPENDIX: KERR EFFECT AND TWO PHOTON ABSORPTION IN A PHOTONIC CRYSTAL

Here we sketch the treatment of two-photon absorption and the Kerr effect (related to the imaginary and real parts of a  $\chi^{(3)}$  interaction, respectively) in a photonic crystal based on the more general formalism developed by Bhat and Sipe,<sup>18</sup> henceforth referred to as BhSi. In that paper the energy flux  $I(\mathbf{r}, t)$  associated with a Bloch mode could be written in terms of a complex slowly varying (in space and time) envelope function  $\psi(\mathbf{r}, t)$  as

$$I(\mathbf{r}, t)\hat{\mathbf{s}} = 2|\psi(\mathbf{r}, t)|^2\hat{\mathbf{s}} = \langle \mathbf{E}(\mathbf{r}, t) \times \mathbf{H}(\mathbf{r}, t) \rangle, \quad (\text{A1})$$

where  $\hat{\mathbf{s}}$  is a unit vector indicating the direction of energy flow in the Bloch mode,  $\langle \rangle$  indicates an average over the rapidly varying time dependence and over a unit cell. Within the usual approximations (no  $\chi^{(2)}$  effects, no degeneracy at the point of interest, etc.) the function  $\psi(\mathbf{r}, t)$  satisfies the equation

$$\frac{\partial \psi(\mathbf{r}, t)}{\partial t} + v^i(\mathbf{k}) \frac{\partial \psi(\mathbf{r}, t)}{\partial r^i} = \frac{1}{2} \frac{\partial^2 \omega(\mathbf{k})}{\partial k^i \partial k^j} \frac{\partial^2 \psi(\mathbf{r}, t)}{\partial r^i \partial r^j} + i\omega(\mathbf{k})\sigma\psi(\mathbf{r}, t) + i \frac{\alpha}{\epsilon_0 v(\mathbf{k})} \psi(\mathbf{r}, t) |\psi(\mathbf{r}, t)|^2. \quad (\text{A2})$$

Here  $\mathbf{v}(\mathbf{k})$  [with Cartesian component  $v^i(\mathbf{k})$ ] is the group velocity, the term involving  $\partial^2 \omega(\mathbf{k}) / \partial k^i \partial k^j$  describes both diffraction and group velocity dispersion, the coefficient  $\sigma$  describes linear loss, and  $\alpha$  describes the  $\chi^{(3)}$  interaction. All functions of  $\mathbf{k}$  are evaluated at the  $\mathbf{k}$  of the modulated Bloch function. We have taken the  $\chi^{(3)}$  nonlinearity to be described as

$$P_{NL}^i(\mathbf{r}, t) = 3\varepsilon_0 \chi_3^{ijkl}(\mathbf{r}; -\omega; \omega, \omega, -\omega) \mathcal{E}^j(\mathbf{r}, t) \mathcal{E}^k(\mathbf{r}, t) \\ \times [\mathcal{E}^l(\mathbf{r}, t)]^* e^{-i\omega t} + \text{c.c.},$$

where  $\omega$  is the carrier frequency of the pulse [ $\omega \equiv \omega(\mathbf{k})$ ] and  $\mathbf{E}(\mathbf{r}, t) = \mathcal{E}(\mathbf{r}, t)e^{-i\omega t} + \text{c.c.}$  With these definitions,  $\alpha$  is given by

$$\alpha = \frac{3}{2} \omega \int_{\text{cell}} \frac{d\mathbf{r}}{\Omega_{\text{cell}}} \chi_3^{ijkl}(\mathbf{r}; -\omega; \omega, \omega, -\omega) [E_{m\mathbf{k}}^i(\mathbf{r})]^* [E_{m\mathbf{k}}^j(\mathbf{r})] \\ \times [E_{m\mathbf{k}}^k(\mathbf{r})] [E_{m\mathbf{k}}^l(\mathbf{r})]^*, \quad (\text{A3})$$

where  $\Omega_{\text{cell}}$  is the volume of the unit cell and  $\mathbf{E}_{m\mathbf{k}}(\mathbf{r})$  is the Bloch function electric field of the mode  $m\mathbf{k}$  that the envelope function modulates. Here, following BhSi, the Bloch functions are normalized according to

$$\int_{\text{cell}} \frac{d\mathbf{r}}{\Omega_{\text{cell}}} n^2(\mathbf{r}) \mathbf{E}_{m\mathbf{k}}^*(\mathbf{r}) \cdot \mathbf{E}_{m\mathbf{k}}(\mathbf{r}) = 1,$$

where the first integral is over the normalization volume.

Note that the factor of the group speed  $v(\mathbf{k})$  in the denominator of Eq. (A2) arises because the nonlinearity  $\chi^{(3)}$  is referenced to the electric field amplitude, while Eq. (A2) is an equation for the intensity amplitude, and for a given intensity  $I(\mathbf{r}, t) \hat{=} 2|\psi(\mathbf{r}, t)|^2 \hat{=} 2$  the electric field amplitude is greater the more slowly the field is propagating. We pick up a second factor of the group velocity, which can be seen most easily by examining a field that is propagating precisely at the carrier frequency  $\omega$ , for which the slowly varying amplitude  $\psi(\mathbf{r}, t)$  has no time dependence. Neglecting diffraction and dispersion effects, and setting  $\sigma=0$  (no linear absorption, etc.), Eq. (A2) reduces to

$$v(\mathbf{k}) \frac{\partial \psi(z, t)}{\partial z} = i \frac{\alpha}{\varepsilon_0 v(\mathbf{k})} \psi(z, t) |\psi(z, t)|^2, \quad (\text{A4})$$

where we now assume that the field propagates in the  $z$  direction in the crystal, which we take to be the direction  $\mathbf{k}$  of the modulated Bloch function. This equation is trivially written as

$$\frac{\partial \psi(z, t)}{\partial z} = i \frac{\alpha}{\varepsilon_0 v^2(\mathbf{k})} \psi(z, t) |\psi(z, t)|^2. \quad (\text{A5})$$

So now there is indeed a second factor of  $v(\mathbf{k})$  in the denominator; this one arises because, colloquially speaking, the nonlinearity is more effective the slower the group velocity because the light spends “more time” sampling the nonlinearity.

The real part of  $\alpha$  describes the intensity-dependent index of refraction and the imaginary part describes 2PA. For example, using Eq. (A1), we find from Eq. (A5) that

$$\frac{\partial I(z)}{\partial z} = -\beta I^2(z),$$

where

$$\beta = \frac{\text{Im}(\alpha)}{\varepsilon_0 v^2(\mathbf{k})} \quad (\text{A6})$$

is the phenomenological 2PA absorption coefficient associated with the Bloch function  $\mathbf{E}_{m\mathbf{k}}(\mathbf{r})$ . Thus, in place of Eq. (A3) we can write

$$\alpha = \frac{3}{2} \omega \frac{\int_{\text{cell}} \frac{d\mathbf{r}}{\Omega_{\text{cell}}} \chi_3^{ijkl}(\mathbf{r}; -\omega; \omega, \omega, -\omega) [E_{m\mathbf{k}}^i(\mathbf{r})]^* [E_{m\mathbf{k}}^j(\mathbf{r})] [E_{m\mathbf{k}}^k(\mathbf{r})] [E_{m\mathbf{k}}^l(\mathbf{r})]^*}{\left( \int_{\text{cell}} \frac{d\mathbf{r}}{\Omega_{\text{cell}}} n^2(\mathbf{r}) \mathbf{E}_{m\mathbf{k}}^*(\mathbf{r}) \cdot \mathbf{E}_{m\mathbf{k}}(\mathbf{r}) \right)^2}. \quad (\text{A7})$$

This is a more convenient way to write  $\alpha$ , because it is now unmodified by a change in whatever normalization condition is adopted for  $\mathbf{E}_{m\mathbf{k}}(\mathbf{r})$ . Hence,  $\mathbf{E}_{m\mathbf{k}}(\mathbf{r})$  can be taken directly from any technique that finds the Bloch functions. From the symmetry properties of  $\chi_3^{ijkl}(\mathbf{r}; -\omega; \omega, \omega, -\omega)$  we only get an imaginary part of  $\alpha$  from an imaginary part of  $\chi_3^{ijkl}(\mathbf{r}; -\omega; \omega, \omega, -\omega)$ ; hence combining Eq. (11) and Eq. (12), we find

$$\beta = \frac{3\omega}{2\varepsilon_0 v^2(\mathbf{k})} \frac{\int_{\text{cell}} \frac{d\mathbf{r}}{\Omega_{\text{cell}}} \text{Im}[\chi_3^{ijkl}(\mathbf{r}; -\omega; \omega, \omega, -\omega)] [E_{m\mathbf{k}}^i(\mathbf{r})]^* [E_{m\mathbf{k}}^j(\mathbf{r})] [E_{m\mathbf{k}}^k(\mathbf{r})] [E_{m\mathbf{k}}^l(\mathbf{r})]^*}{\left( \int_{\text{cell}} \frac{d\mathbf{r}}{\Omega_{\text{cell}}} n^2(\mathbf{r}) \mathbf{E}_{m\mathbf{k}}^*(\mathbf{r}) \cdot \mathbf{E}_{m\mathbf{k}}(\mathbf{r}) \right)^2}. \quad (\text{A8})$$

Once the Bloch function of interest is known, and a model for  $\chi_3^{ijkl}(\mathbf{r}; -\omega; \omega, \omega, -\omega)$  adopted, then it is only two integrals over the unit cell that must be done to find  $\beta$ , once  $v(\mathbf{k})$  is determined from the band structure.

One can verify the above expression for a uniform, bulk medium. To do that, we imagine a plane wave propagating along the  $z$  direction so that

$$\mathbf{E}_{m\mathbf{k}}(\mathbf{r}) \rightarrow \hat{\mathbf{e}}e^{ikz},$$

where  $\hat{\mathbf{e}}$  is a polarization direction, and is perpendicular to  $\hat{\mathbf{z}}$ . Here we have  $v(\mathbf{k})=c/n$ , where  $n$  is the uniform index of refraction, and from Eq. (A8) we get

$$\beta = \frac{3\omega}{2\varepsilon_0 c^2 n^2} \text{Im}[\chi_3^{eeee}(-\omega; \omega, \omega, -\omega)],$$

where now  $\chi_3^{eeee}(-\omega; \omega, \omega, -\omega)$  is the indicated component of a uniform  $\chi_3$ .

Now consider the phenomenological description of light propagation through this material, with an  $n_2=n_2^R+in_2^I$  that has both a real and imaginary part, as indicated. A wave propagates as

$$\exp\left(i\frac{\omega}{c}(n_2 I)z\right) = \exp\left(i\frac{\omega}{c}(n_2^R)z\right) \exp\left(-\frac{\omega}{c}(n_2^I)z\right),$$

which gives an intensity dropping off as

$$\exp\left(-\frac{\omega}{c}(2n_2^I)z\right),$$

and so we can identify a phenomenological

$$\beta^{bulk} = \frac{2\omega}{c}n_2^I.$$

Since we have

$$n_2 = \frac{3}{4\varepsilon_0 c n^2} \chi_3^{eeee}(-\omega; \omega, \omega, -\omega)$$

for this geometry [see BhSi, Eq. (122)], we have

$$\beta = \beta^{bulk},$$

as expected.

The expression (A8) can be simplified for common situations. For example, if the PhC has two constituents with one of them air (for which we neglect 2PA) and the other a solid, then the integration in the numerator of Eq. (A8) only has to be performed over the solid. Furthermore, if the solid has cubic symmetry for the electronic lattice and the beam is polarized along a cubic axis then the 2PA coefficient for this mode is

$$\beta = \beta^{bulk} \frac{c^2}{v^2(\mathbf{k})} \frac{\int_{cell'} \frac{d\mathbf{r}}{\Omega_{cell}} n^2(\mathbf{r}) |E_{m\mathbf{k}}(\mathbf{r})|^4}{\left( \int_{cell} \frac{d\mathbf{r}}{\Omega_{cell}} n^2(\mathbf{r}) \mathbf{E}_{m\mathbf{k}}^*(\mathbf{r}) \cdot \mathbf{E}_{m\mathbf{k}}(\mathbf{r}) \right)^2}, \quad (\text{A9})$$

where the  $'$  indicates that the integration is only over the solid region of the unit cell and  $\beta^{bulk}$  is the 2PA coefficient for the solid for the assumed beam polarization. From this last equation and for the purposes of generating, e.g., a local carrier generation or energy deposition rate, we can infer a local effective 2PA coefficient given by

$$\beta(\mathbf{r}) = \beta^{bulk} \frac{c^2}{v^2(\mathbf{k})} \frac{n^2(\mathbf{r}) |E_{m\mathbf{k}}(\mathbf{r})|^4}{\left( \int_{cell} \frac{d\mathbf{r}}{\Omega_{cell}} n^2(\mathbf{r}) \mathbf{E}_{m\mathbf{k}}^*(\mathbf{r}) \cdot \mathbf{E}_{m\mathbf{k}}(\mathbf{r}) \right)^2}. \quad (\text{A10})$$

<sup>1</sup>N. Susa, Jpn. J. Appl. Phys., Part 1 **39**, 6288 (2000).

<sup>2</sup>A. Hache and M. Bourgeois, Appl. Phys. Lett. **77**, 4089 (2000).

<sup>3</sup>P. M. Johnson, A. F. Koenderink, and W. L. Vos, Phys. Rev. B **66**, 081102(R) (2002).

<sup>4</sup>S. W. Leonard, H. M. van Driel, J. Schilling, and R. B. Wehrspohn, Phys. Rev. B **66**, 161102(R) (2002).

<sup>5</sup>A. D. Bristow, W. H. Fan, A. M. Fox, M. S. Skolnick, D. M. Whittaker, A. Tahraomi, T. F. Krauss, and J. S. Roberts, Appl. Phys. Lett. **83**, 851 (2003).

<sup>6</sup>D. A. Mazurenko, R. Kerst, J. I. Dijkhuis, A. V. Akimov, V. G. Golubev, D. A. Kurdyukov, A. B. Pevtsov, A. V. Selkin, Phys. Rev. Lett. **91**, 213903 (2003).

<sup>7</sup>Z.-Y. Li, X. Zhang, and Z.-Q. Zhang, Phys. Rev. B **61**, 15738 (2000).

<sup>8</sup>T. Baba, K. Inoshita, H. Tanaka, J. Yonekura, M. Ariga, A. Matsutani, T. Miyamoto, F. Koyama, and K. Iga, J. Lightwave Technol. **17**, 2113 (1999).

<sup>9</sup>G. von Freymann, W. Koch, D. C. Meisel, M. Wegener, M. Diem, A. Garcia-Martin, S. Pereira, K. Busch, J. Schilling, R. B. Wehrspohn, and U. Gösele, Appl. Phys. Lett. **83**, 614 (2003).

<sup>10</sup>H. Kosaka, T. Kawashima, A. Tomita, M. Notomi, T. Tamamura, T. Sato, and S. Kawakami, Phys. Rev. B **58**, R10096 (1998).

<sup>11</sup>T. Tanaka, A. Harata, and T. Sawada, J. Appl. Phys. **82**, 4033 (1997).

<sup>12</sup>C. M. Li, T. Sjödin, and H. L. Dai, Phys. Rev. B **56**, 15252 (1997).

<sup>13</sup>J. Linnros and V. Grivickas, Phys. Rev. B **50**, 16943 (1994).

<sup>14</sup>U. Grüning, V. Lehman, and C. M. Engelhardt, Appl. Phys. Lett. **66**, 3254 (1995).

<sup>15</sup>Note that the group velocities for pulses launched along the  $z$  and  $y$  directions are  $0.29c$  and  $0.31c$ , respectively, close to that in bulk silicon.

<sup>16</sup>W. H. Press, W. T. Vetterling, and S. A. Teukolsky, *Numerical Recipes in C* (Cambridge University Press, Cambridge, UK, 1992).

<sup>17</sup>We have also considered thermal contributions in our simulations but find their influence to be negligible. This is because of the small thermo-optic coefficient of silicon at the probe wavelength ( $dn/dT=2 \times 10^{-4} \text{ K}^{-1}$ ) and the relatively slow recombination velocity of the PhC sample.

- <sup>18</sup>N. A. R. Bhat and J. E. Sipe, *Phys. Rev. E* **64**, 056604 (2001).
- <sup>19</sup>S. W. Leonard, H. M. van Driel, K. Busch, S. John, A. Birner, A.-P. Li, F. Muller, U. Gösele, and V. Lehmann, *Appl. Phys. Lett.* **75**, 3063 (1999).
- <sup>20</sup>A. J. Sabbah and D. M. Riffe, *J. Appl. Phys.* **88**, 6954 (2000).
- <sup>21</sup>Over the experimental time window of 70 ps, the characteristic carrier diffusion length is only 0.26  $\mu\text{m}$  so carrier diffusion out of the probe region can be neglected.
- <sup>22</sup>H. W. Tan, H. M. van Driel, S. L. Schweizer, R. B. Wehrspohn, and U. Gösele, *Phys. Rev. B* **70**, 205110 (2004).
- <sup>23</sup>N. J. Halas and J. Bokor, *Phys. Rev. Lett.* **62**, 1679 (1989).
- <sup>24</sup>S. Jeong and J. Bokor, *Phys. Rev. B* **59**, 4943 (1999).
- <sup>25</sup>Because the pump and probe pulses are signal and idler beams from an OPA we are unable to tune the pump wavelength to 1.25  $\mu\text{m}$  for a probe wavelength of 1.9  $\mu\text{m}$ .